Supplementary Materials

Improving the pore properties of porous aromatic frameworks in two aspects via partition strategy

Hengtao Lei, Zhaofu Zhang, Yuhui Zhai, Xueyan Han, Jian Song, Yue Li*, Yuyang Tian*

Key Laboratory of Polyoxometalate and Reticular Material Chemistry of Ministry of Education, Faculty of Chemistry, Northeast Normal University, Changchun 130024, Jilin, China.

***Correspondence to:** Prof. Yuyang Tian, Dr. Yue Li, Key Laboratory of Polyoxometalate and Reticular Material Chemistry of Ministry of Education, Faculty of Chemistry, Northeast Normal University, 5268 Renmin Street, Changchun 130024, Jilin, China. E-mail: tianyy100@nenu.edu.cn; liy225@nenu.edu.cn

Table of Contents

Supplementary Section 1. Materials and Characterizations

All the reagents were purchased from commercial sources without further purification.

Fourier transform infrared spectroscopy (FTIR). The FT-IR spectra (KBr)were performed on the Nicolet-410 FT-IR spectrophotometer.

^{13}C NMR Solid-state NMR were recorded on Bruker Avance III model 400 MHz NMR spectrometer at a MAS rate of 5 kHz.

Scanning electron microscopy (SEM). Scanning electron microscopy (SEM) was performed on a HITACHI SU8010 microscope instrument. Samples were prepared by ultrasonically dispersing the material in ethanol, dropping it on a silicon wafer and drying it, and then coated with gold.

Nitrogen isotherm measurements. Nitrogen sorption experiments were performed at 77 K up to 1 bar using a nanometric sorption analyzer. The adsorption–desorption isotherms of N_2 were obtained at 77 K using a an Autosorb iQ2 adsorptometer, Quantachrome Instrument. Before sorption analysis, the sample was evacuated at 100 ^{o}C for 10 h using a turbomolecular vacuum pump. Specific surface areas were calculated from nitrogen adsorption data by multipoint BET analysis.

Thermogravimetric analysis (TGA). Thermogravimetric analysis (TGA) was measured on the Mettler Toledo thermal analyzer in the temperature range of 30–800 °C with a heating rate of 10℃ min^{-1} under an air flow.

UV-Vis spectra analysis. The UV-Vis spectra were measured through the Cary 500 UV-Visible spectrophotometer.

Supplementary Section 2. Synthetic Procedure

2.1 Preparation of PAF-11

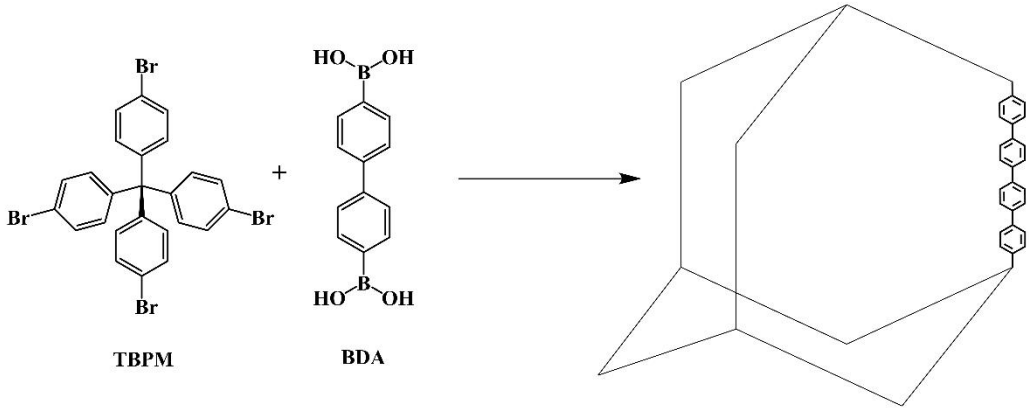

A 100 mL two-neck round bottom flask were charged with tetra(4-bromophenyl)methane (TBPM,0.248 g, 0.39 mmol), 4,4'-biphenyldiboronic acid (BDA, 0.188 g, 0.78 mmol) and tetrakis(triphenylphosphine) palladium (0) (0.045 g, 0.04 mmol) under nitrogen atmosphere. Then, 12 mL N, N'-dimethylformamide (DMF) and potassium carbonate (1.5 mL, 2 M, 3.00 mmol) were quickly added in the mixture under continuous nitrogen, and degassed by three freeze–pump–thaw cycles. The mixture was stirred and heated to 150℃ for 24 h. After cooling to room temperature, the product was filtered and washed with DMF (120 mL*2), H_2O (120 mL*2), THF (120 mL*2) and EtOH (120 mL) to remove the catalyst and unreacted monomers. Lastly, the product was dried under vacuum at 100℃ for 8 h to yield off-white powder (224 mg, yield = 93%).

2.2 Preparation of PAF-140

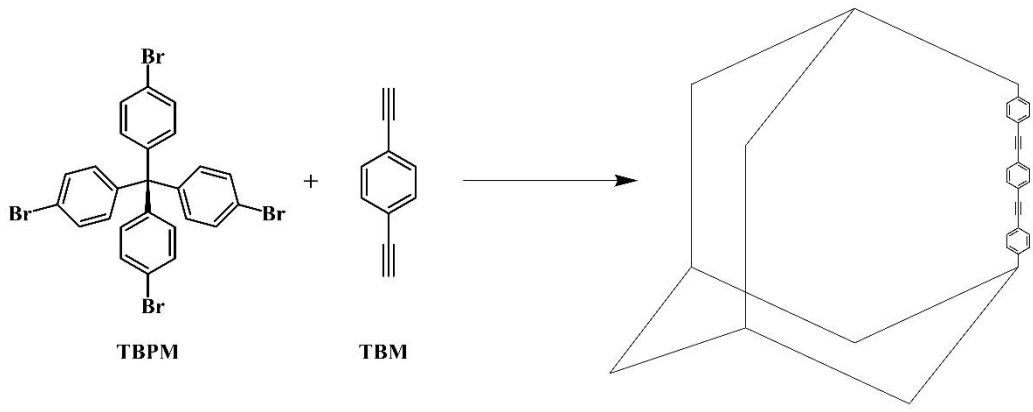

A 100 mL two-neck round bottom flask was charged with tetra(4-bromophenyl)methane (TBPM, 0.254 g, 0.40 mmol) under nitrogen atmosphere.

Then, 1,4-diethynylbenzene (DEB, 0.101 g, 0.80 mmol) , tetrakis(triphenylphosphine) palladium (0) (0.030 g, 0.03mmol) , copper(I) iodide (0.010 g, 0.05 mmol) , 15 mL DMF and 15 mL triethylamine were quickly added under continuous nitrogen, and degassed by three freeze–pump–thaw cycles. The mixture stirred and heated to 100℃ for 48 h. After cooling to room temperature, the product was filtered and washed with 6 mol L^{-1} HCl (120 mL*2), H_2O (120 mL*2), and CH_2Cl_2 (120 mL*2) to remove the catalyst and unreacted monomers. Then, the product was then further purified by Soxhlet extraction with THF for 36 h. Lastly, the product was dried under vacuum at 100℃ for 8 h to yield yellow powder (208 mg, yield = 92%).

2.3 Preparation of partitioning PAFs

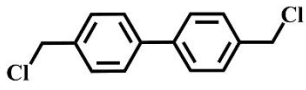

PCBP

PAF-11-p1: PAF-11 (0.100 g), 4,4’-bis(chloromethyl)-1,1’-biphenyl (0.026 g, 0.10 mmol), $FeCl_3$ (0.033 g, 0.20 mmol) and 1,2-dichloroethane (12 mL) was stirred at 85℃ for 16 h in 50 mL two-neck round bottom flask under nitrogen atmosphere. Upon completion. The reaction was quenched with MeOH. Then, the mixture was filtered and washed with THF (120 mL), 6 mol L^{-1} HCl (120 mL*2), H_2O (120 mL*2), and ETOH (120 mL). Lastly, the product was dried under vacuum at 100℃ for 8 h to yield gray-yellow powder (0.115 g, yield = 96%).

PAF-11-2: PAF-11 (0.100 g), 4,4’-bis(chloromethyl)-1,1’-biphenyl (0.051 g, 0.20 mmol), $FeCl_3$ (0.066 g, 0.40 mmol) and 1,2-dichloroethane (12 mL) were stirred at 85℃ for 16 h in 50 mL two-neck round bottom flask under nitrogen atmosphere. Upon completion. The reaction was quenched with MeOH. Then, the mixture was filtered and washed with THF (120 mL), 6 mol L^{-1} HCl (120 mL*2), H_2O (120 mL*2), and ETOH (120 mL). Lastly, the product was dried under vacuum at 100℃ for 8 h to yield gray-yellow powder (0.130 g, yield = 95%).

PAF-11-p3: PAF-11 (0.100 g), 4,4’-bis(chloromethyl)-1,1’-biphenyl (0.077 g, 0.30 mmol), $FeCl_3$ (0.099 g, 0.60 mmol) and 1,2-dichloroethane (12 mL) were stirred at 85℃ for 16 h in 50 mL two-neck round bottom flask under nitrogen atmosphere. Upon completion. The reaction was quenched with MeOH. Then, the mixture was filtered

and washed with THF (120 mL), 6 mol L^{-1} HCl (120 mL*2), H_2O (120 mL*2), and ETOH (120 mL). Lastly, the product was dried under vacuum at 100℃ for 8 h to yield gray-yellow powder (0.149 g, yield = 96%).

PAF-11-p4: PAF-11 (0.100 g), 4,4'-bis(chloromethyl)-1,1'-biphenyl (0.102 g, 0.40 mmol), $FeCl_3$ (0.132 g, 0.80 mmol) and 1,2-dichloroethane (12 mL) were stirred at 85℃ for 16 h in 50 mL two-neck round bottom flask under nitrogen atmosphere. Upon completion. The reaction was quenched with MeOH. Then, the mixture was filtered and washed with THF (120 mL), 6 mol L^{-1} HCl (120 mL*2), H_2O (120 mL*2), and ETOH (120 mL). Lastly, the product was dried under vacuum at 100℃ for 8 h to yield gray-yellow powder (0.164 g, yield = 95%).

PAF-140-p1: PAF-140 (0.100 g), 4,4'-bis(chloromethyl)-1,1'-biphenyl (0.033g, 0.13 mmol), $FeCl_3$ (0.042 g, 0.26 mmol) and 1,2-dichloroethane (12 mL) were stirred at 85℃ for 16 h in 50 mL two-neck round bottom flask under nitrogen atmosphere. Upon completion. The reaction was quenched with MeOH. Then, the mixture was filtered and washed with THF (120 mL), 6 mol L^{-1} HCl (120 mL*2), H_2O (120 mL*2), and ETOH (120 mL). Lastly, the product was dried under vacuum at 100℃ for 8 h to yield yellow-brown powder (0.120 g, yield = 97%).

PAF-140-p2: PAF-140 (0.100 g), 4,4'-bis(chloromethyl)-1,1'-biphenyl (0.065g, 0.26 mmol), $FeCl_3$ (0.084 g, 0.52 mmol) and 1,2-dichloroethane (12 mL) were stirred at 85℃ for 16 h in 50 mL two-neck round bottom flask under nitrogen atmosphere. Upon completion. The reaction was quenched with MeOH. Then, the mixture was filtered and washed with THF (120 mL), 6 mol L^{-1} HCl (120 mL*2), H_2O (120 mL*2), and ETOH (120 mL). Lastly, the product was dried under vacuum at 100℃ for 8 h to yield yellow-brown powder (0.140 g, yield = 95%).

PAF-140-p3: PAF-140 (0.100 g), 4,4'-bis(chloromethyl)-1,1'-biphenyl (0.098g, 0.39 mmol), $FeCl_3$ (0.126 g, 0.78 mmol) and 1,2-dichloroethane (12 mL) were stirred at 85℃ for 16 h in 50 mL two-neck round bottom flask under nitrogen atmosphere. Upon completion. The reaction was quenched with MeOH. Then, the mixture was filtered and washed with THF (120 mL), 6 mol L^{-1} HCl (120 mL*2), H_2O (120 mL*2), and ETOH (120 mL). Lastly, the product was dried under vacuum at 100℃ for 8 h to yield yellow-brown powder (0.159 g, yield = 93%).

PAF-140-p4 PAF-140 (0.100 g), 4,4'-bis(chloromethyl)-1,1'-biphenyl (0.130g, 0.52 mmol), $FeCl_3$ (0.168 g, 0.10 mmol) and 1,2-dichloroethane (12 mL) were stirred at

85℃ for 16 h in 50 mL two-neck round bottom flask under nitrogen atmosphere. Upon completion. The reaction was quenched with MeOH. Then, the mixture was filtered and washed with THF (120 mL), 6 mol L^{-1} HCl (120 mL*2), H_2O (120 mL*2), and ETOH (120 mL). Lastly, the product was dried under vacuum at 100℃ for 8 h to yield yellow-brown powder (0.179 g, yield = 93%).

Supplementary Section 3. Fourier-transform infrared spectroscopy

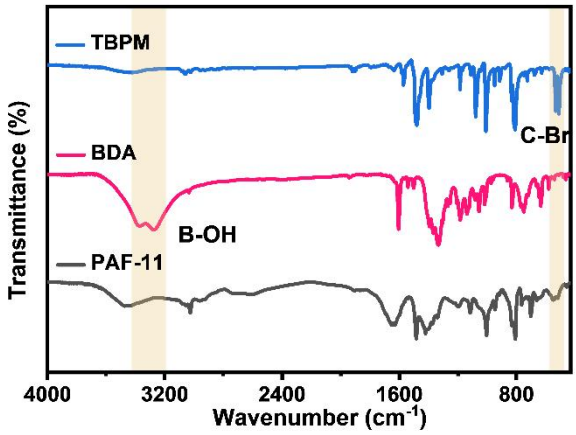

Supplementary Figure 1. FT-IR spectra of PAF-11, TBPM, and BDA for comparison.

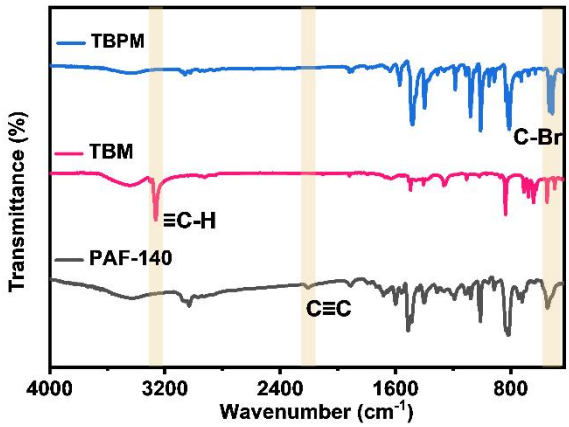

Supplementary Figure 2. FT-IR spectra of PAF-140, TBPM, and TBM for comparison.

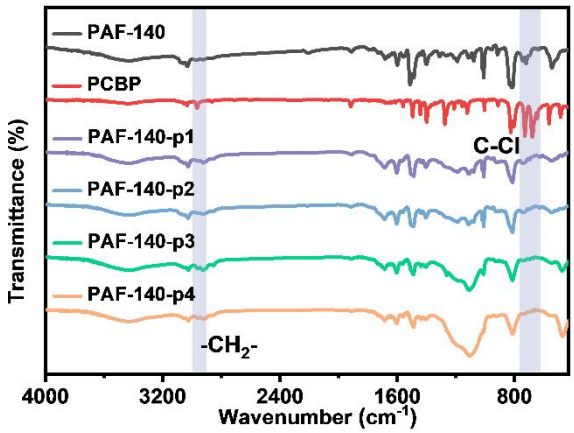

Supplementary Figure 3. FT-IR spectra of PAF-11 and corresponding partitioning PAFs with different pore partition ratios.

Supplementary Section 4. Powder X-ray diffraction

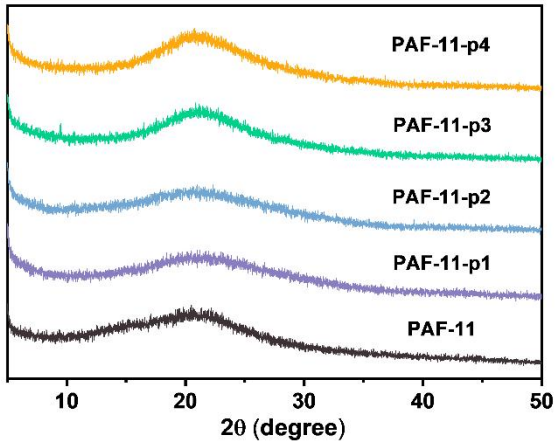

Supplementary Figure 4. PXRD patterns of PAF-11 and corresponding partitioning PAFs with different pore partition ratios.

Supplementary Section 5. SEM image

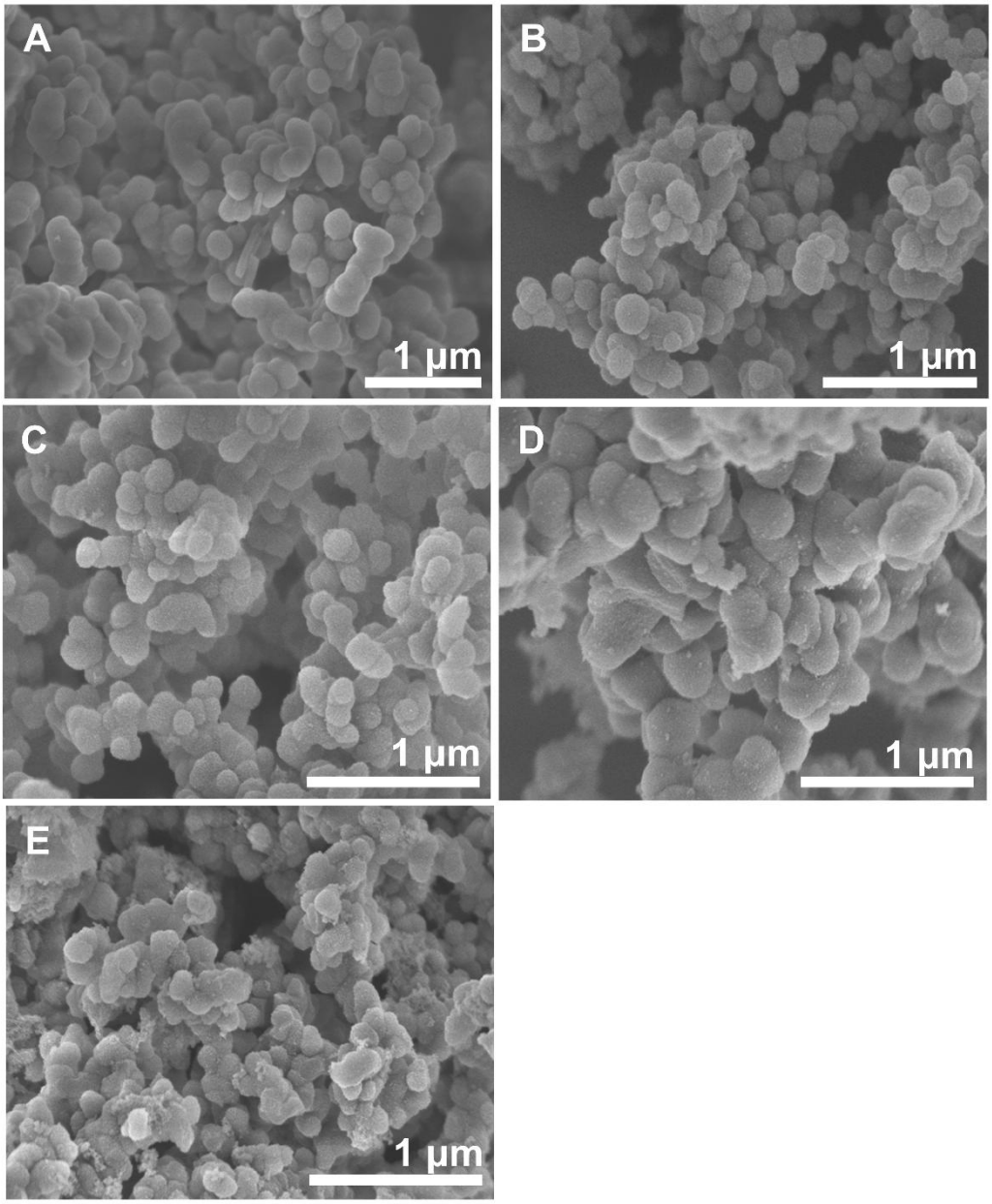

Supplementary Figure 5. SEM images (A-E) of PAF-11 and corresponding partitioning PAFs. scale bars: 1 μm.

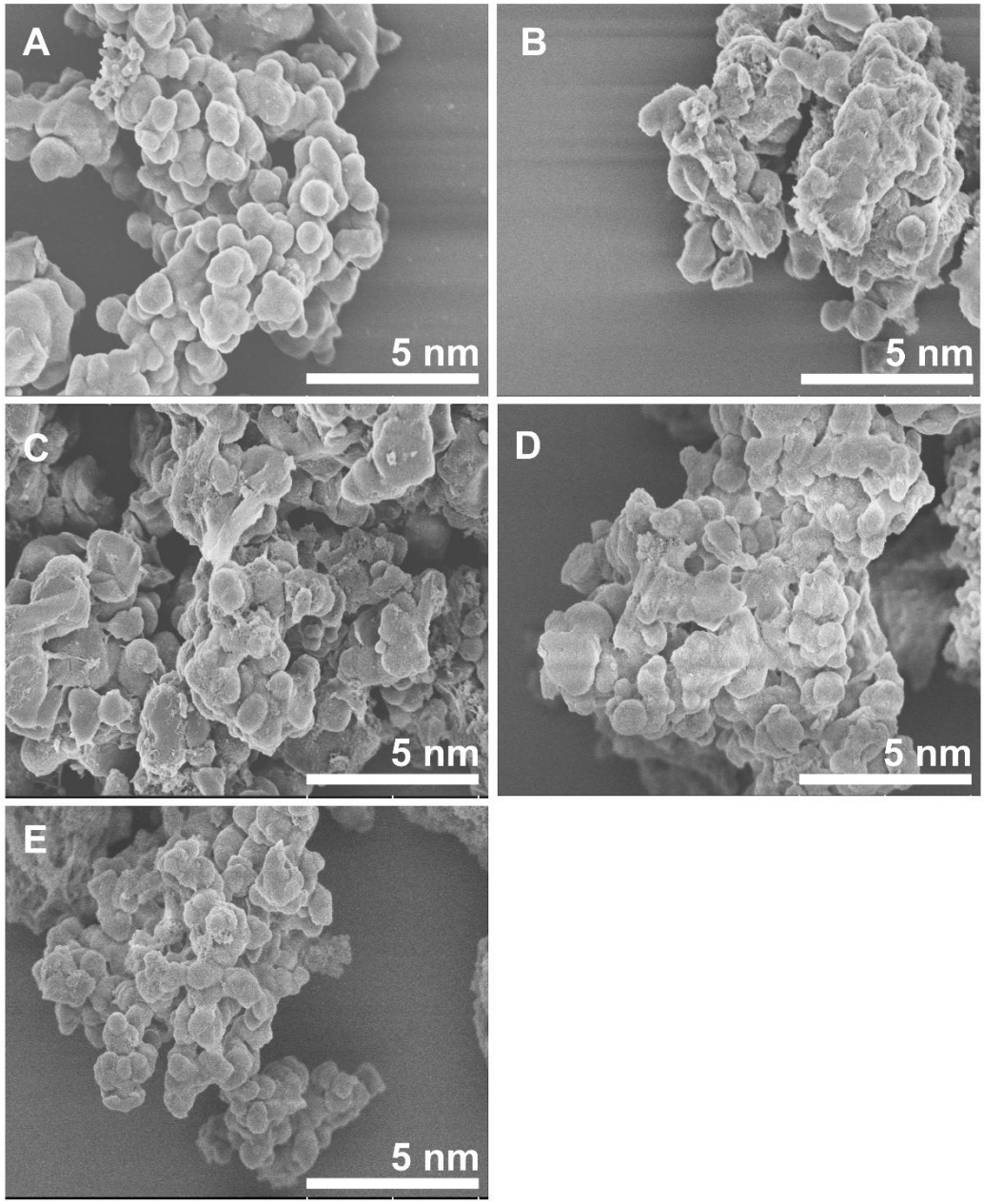

Supplementary Figure 6. SEM images (A-E) of PAF-140 and corresponding partitioning PAFs. scale bars: 5 μm.

Supplementary Section 6. Nitrogen adsorption

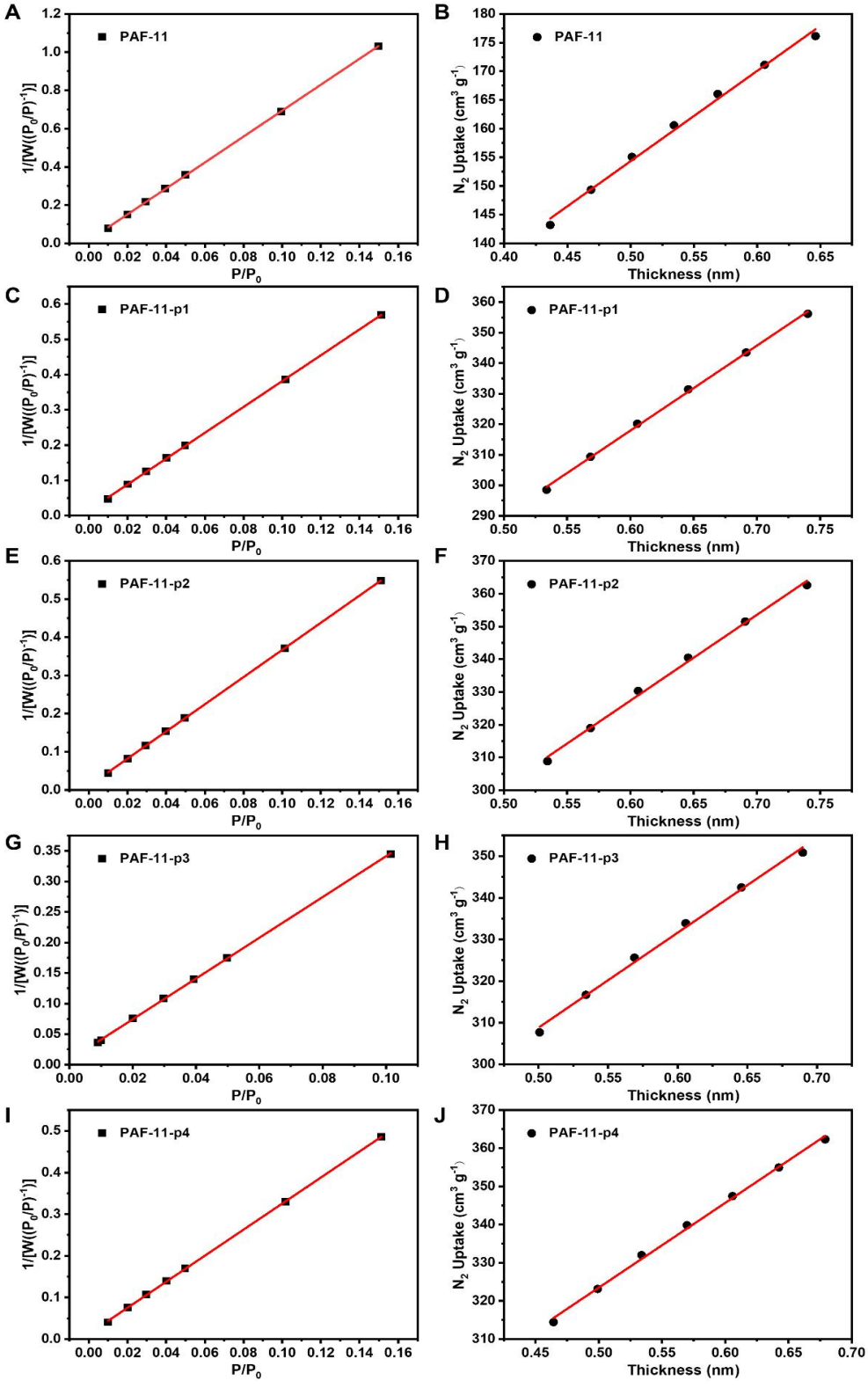

Supplementary Figure 7. Surface area of PAF-11 and corresponding partitioning PAFs calculated using the BET equation (Figures A, C, E, G, I),and micropore surface area calculated using t-plot (Figures B, D, F, H, J).

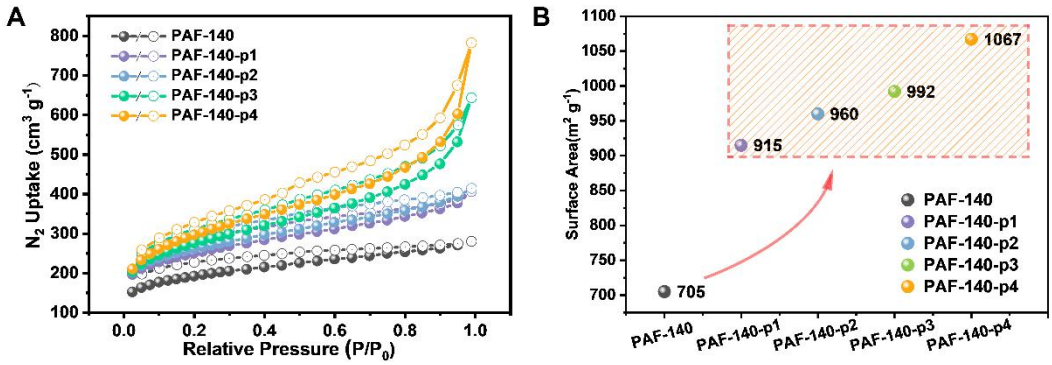

Supplementary Figure 8. (A) Nitrogen-sorption isotherm curves measured at 77 K of PAF-140 and corresponding partitioning PAFs. (B) Variation range of surface area of PAF-140 and corresponding partitioning PAFs..

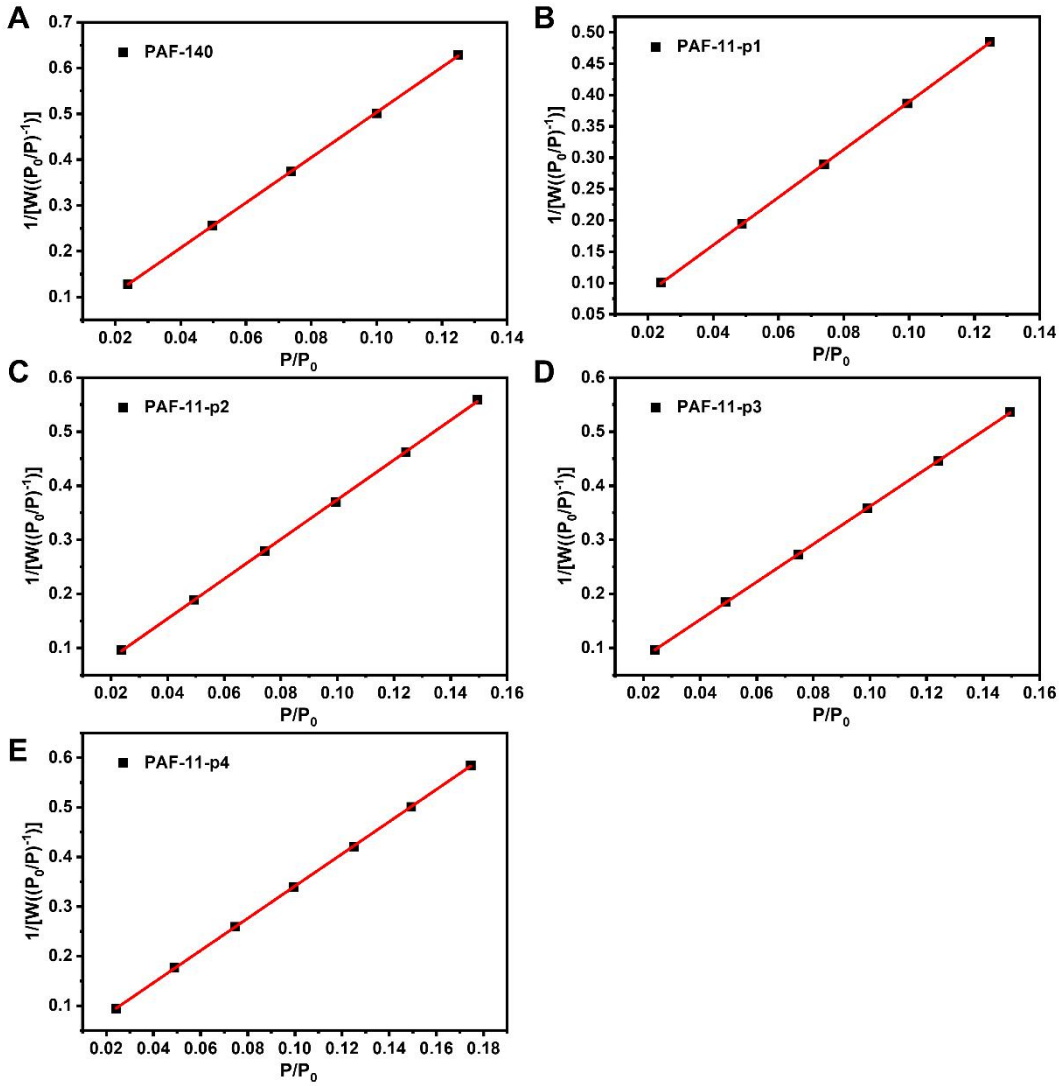

Supplementary Figure 9. Surface area of PAF-140 and corresponding partitioning PAFs calculated using the BET equation.

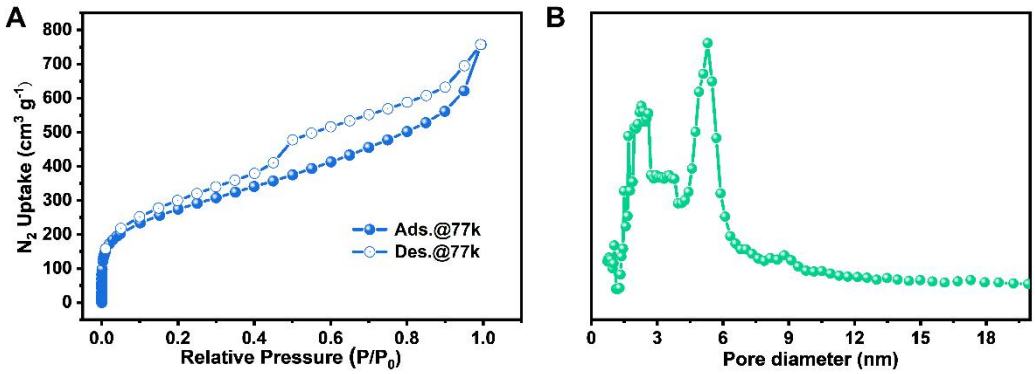

Supplementary Figure 10. (A) Nitrogen-sorption isotherm curves measured at 77 K of PCBP self-polymerization. (B) Pore size distribution of PCBP self-polymerization.

Supplementary Table 1. Composition and pore properties of resulting PAFs.

Sample	**M_{em} (mg)[a]**	**S_{BET} ($m^2\ g^{-1}$) [b]**	**$R_{Surface\ area}$[c]**
PAF-140	-	705	-
PAF-11-1p	0.13	915	130
PAF-140-p2	0.26	960	134
PAF-140-p3	0.39	992	139
PAF-140-p4	0.52	1067	149

[a] Relative to the mole amount of pore partition agent added per 100 mg parent PAF-140. [b] Surface area calculated using the BET equation (Supplementary Figure 8). [c] The rate of increase in micropore volume of partitioning PAFs relative to parent PAF-140.

Supplementary Section 7. TGA curves

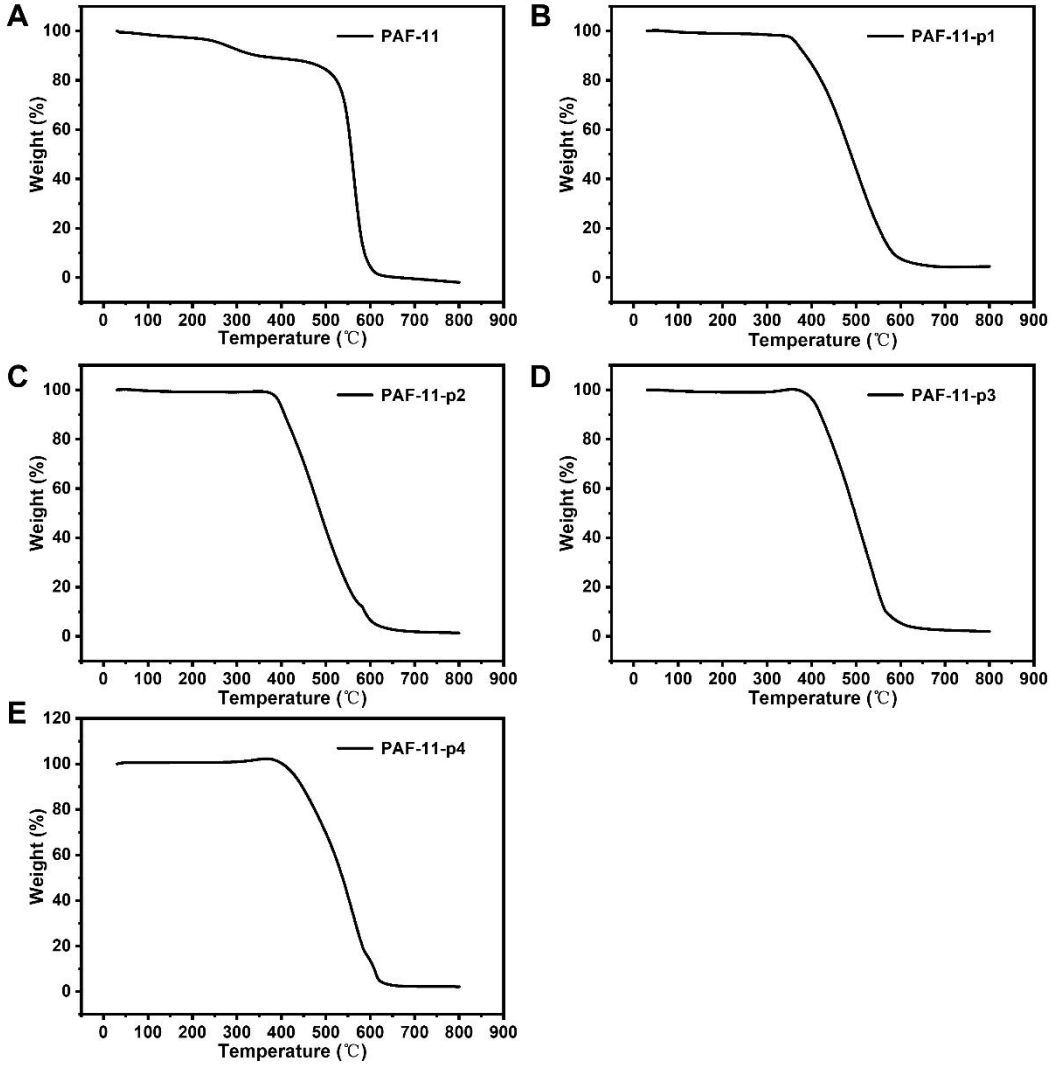

Supplementary Figure 11. TGA plot of PAF-11 and corresponding partitioning PAFs at air condition.

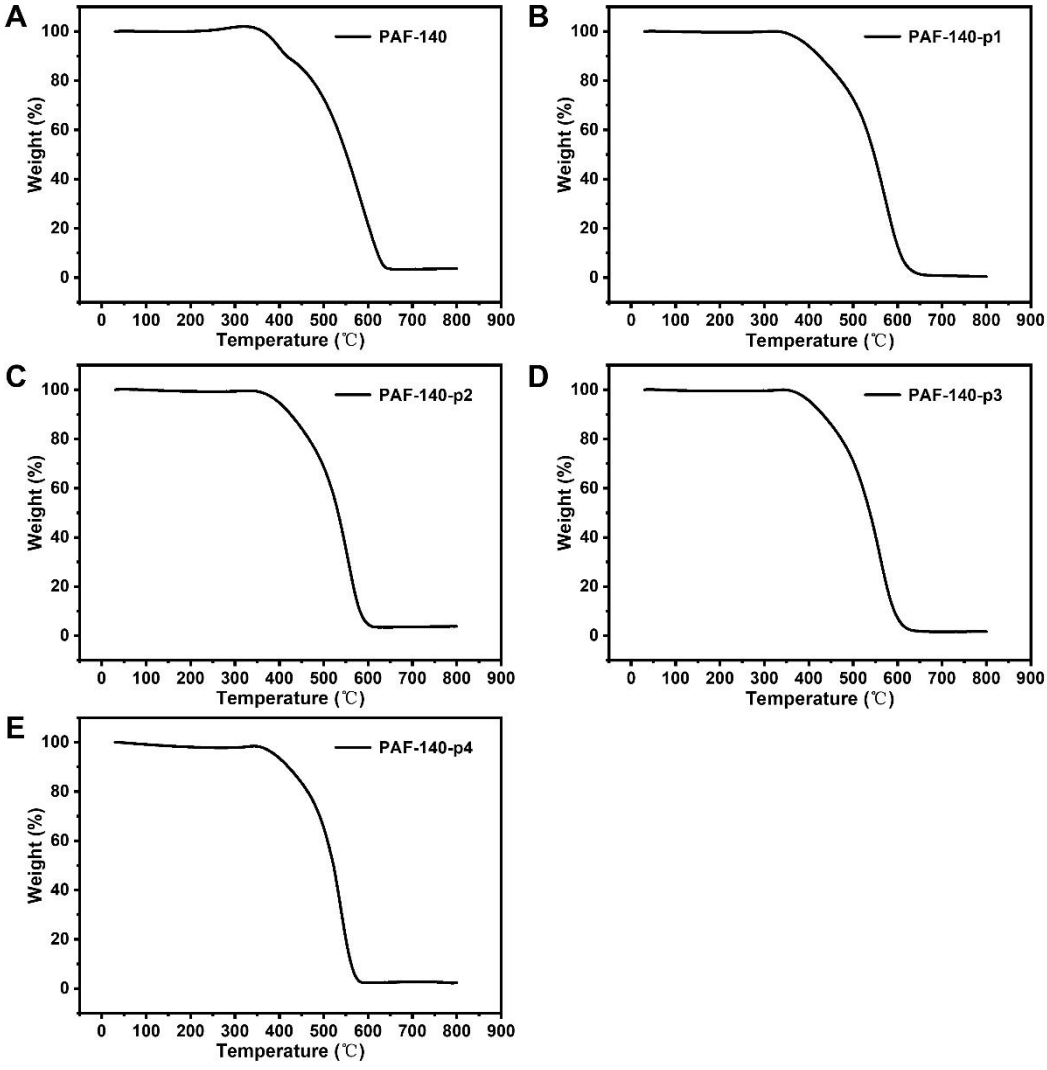

Supplementary Figure 12. TGA plot of PAF-140 and corresponding partitioning PAFs at air condition.

Supplementary Section 8. Chemical stability tests

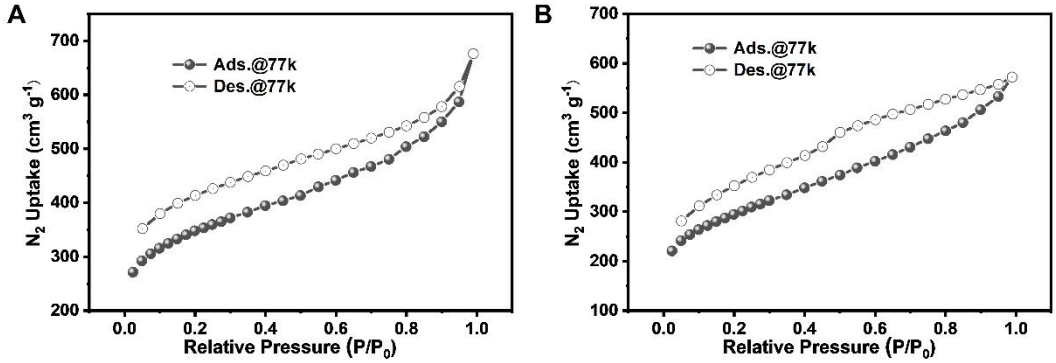

Supplementary Figure 13. Nitrogen-sorption isotherm curves of PAF-11-p4 (A) and PAF-140-p4 (B) after stirring in commonly used organic solvents including tetrahydrofuran, methanol, dichloromethane, ethanol, acetone, chloroform and DMF for 24 hours.

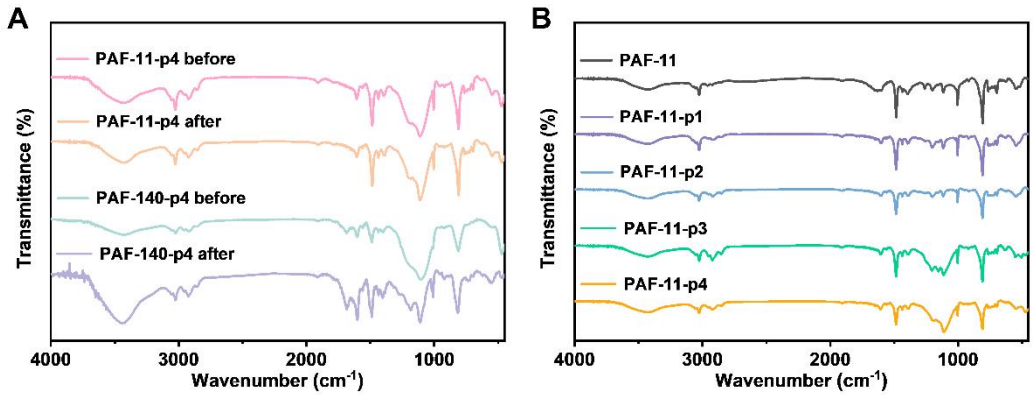

Supplementary Figure 14. FT-IR spectra of (A) PAF-11-p4 and PAF-140-p4, (B) PAF-11 and corresponding partitioning PAFs after stirring in commonly used organic solvents including tetrahydrofuran, methanol, dichloromethane, ethanol, acetone, chloroform and DMF for 24 hours.

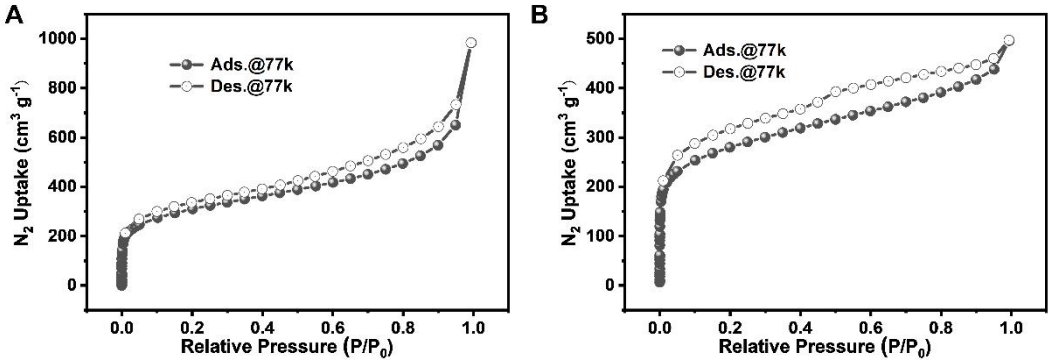

Supplementary Figure 15. Nitrogen-sorption isotherm curves of PAF-11-p4 (A) and PAF-140-p4 (B) after being in normal room air for over a year.

Supplementary Section 9. Carbon dioxide adsorption

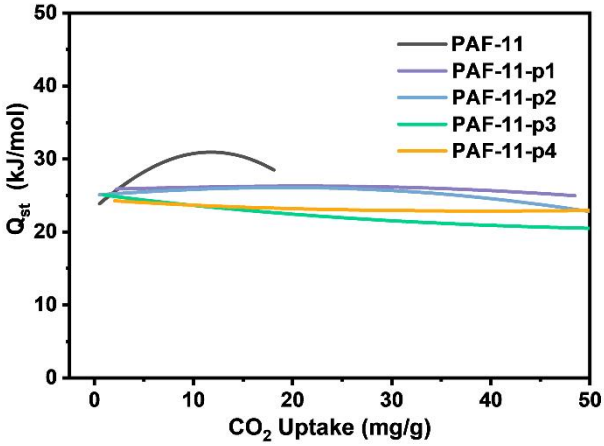

Supplementary Figure 16. Plots of the isosteric heat of adsorption (Q_{st}) for CO_2 and versus CO_2 uptake about PAF-11 and corresponding partitioning PAFs.

Supplementary Section 10. Size-dependent dye adsorption

Dye adsorption study

Studies on adsorption of dye were carried out spectrophotometrically. All the experiments of dye adsorption by PAF-11 and partitioning PAFs were carried out in same conditions. Before adsorption, the adsorbents were dried overnight under vacuum at 100 °C and were kept in a desiccator.

An aqueous stock solution of dye (500 ppm) was prepared by dissolving 500 mg of AB ($C_{37}H_{29}N_3O_9S_3Na_2$, MW:799.8), RB ($C_{28}H_{31}ClN_2O_3$, MW:479.01), MB ($C_{16}H_{20}ClN_3OS$, MW: 337.9) or MO ($C_{14}H_{14}N_3NaO_3S$, MW: 327.34) in deionized water and then making the volume upto 1000 mL. All other subsequent solutions with different concentration of dye (20–400 ppm) were prepared by successive dilution of the stock solution with water. The dye concentrations were determined using an absorbance of the solutions after getting the UV spectra of the solution with a spectrophotometer. A linear relationship was observed between concentration of dye solution and absorbance. The standard curve was obtained from the spectra of the standard solutions (2.5–70 ppm).

The effect of initial dye concentration was studied by using solutions of dye with different concentrations (5 ppm to 500 ppm). 5 mg of PAFs is added in each of these solutions (10 mL). The dye adsorption capacity, i.e. amount of dye (in mg) adsorbed of PAFs per gram (q_e) of adsorbent were calculated according to the following equations:

$$q_e = \frac{(C_0 - C_e)V}{m} \qquad (1)$$

where q_e (mg/g) is the adsorption capacity, C_0 and C_e are the initial and equilibrium concentrations of dye in mg/L, V (L) is the volume of dye solution, and m (g) is the mass of adsorbent used.

Through the adsorption isotherm, the theoretical maximum adsorption capacity and the interaction between the adsorbent and the guest molecule can be known.

The isothermal adsorption curves of dyes were fitted and analyzed by Langmuir and

Freundlich isothermal adsorption models. When it conforms to the Langmuir isothermal adsorption model, it is a single-layer adsorption, and the adsorption sites are uniform. The adsorption active sites have a strong interaction force with the guest molecules. The linear form is as follows:

$$\frac{C_e}{q_e} = \frac{C_e}{q_m} + \frac{1}{q_m K_L} \qquad (2)$$

In the equation, q_e (mg/g) is the same as Equation (1), q_m (mg/g) is the theoretical maximum adsorption capacity of the adsorbent, C_e (mol/L) is the concentration of the system at equilibrium, and K_L (L/mg) is the equilibrium constant.

When it conforms to the Freundlich isothermal adsorption model, it is multi-layer adsorption, and the adsorption sites are uneven. The linear form is as follows :

$$\ln q_e = \ln K_F + \frac{1}{n} \ln C_e \qquad (3)$$

In the equation, K_F (L/mg) is the adsorption capacity constant of the Freundlich isotherm adsorption model, and the value of n is the adsorbent constant. The meanings of q_e and C_e are the same as Equation (2).

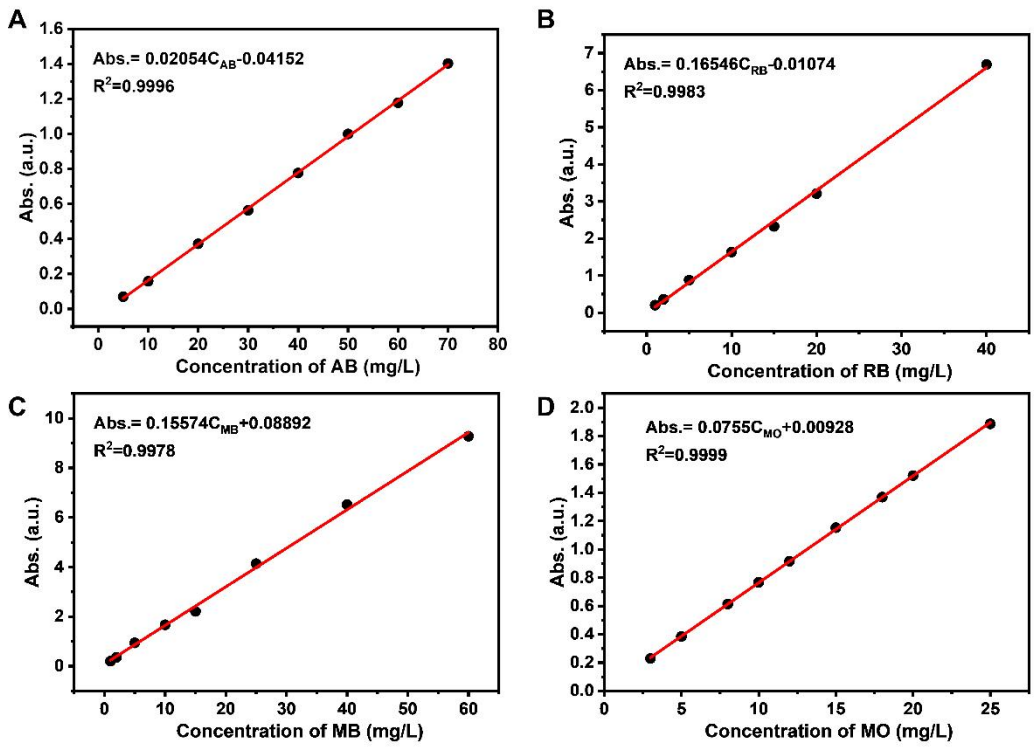

Supplementary Figure 17. Standard Curves for MB, RB, MB and MO.

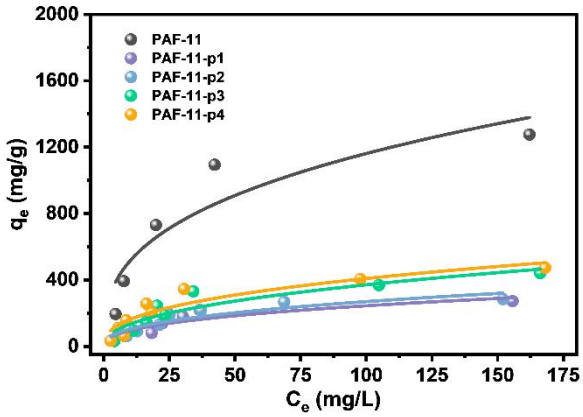

Supplementary Figure 18. AB adsorption isotherms by PAF-11 and corresponding partitioning PAFs analyzed through Freundlich model.

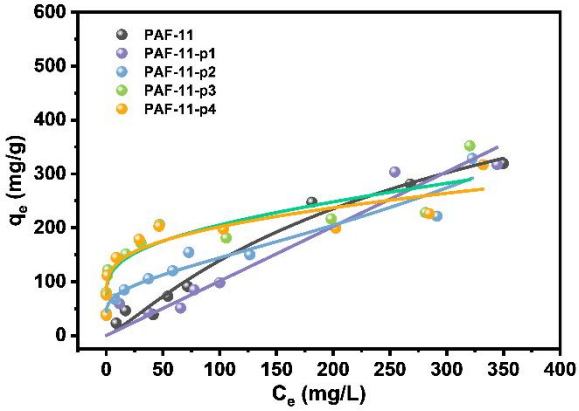

Supplementary Figure 19. RB adsorption isotherms by PAF-11 and corresponding partitioning PAFs analyzed through Freundlich model.

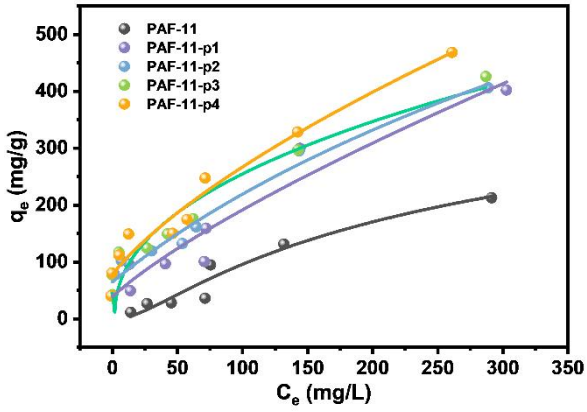

Supplementary Figure 20. MB adsorption isotherms by PAF-11 and corresponding partitioning PAFs analyzed through Freundlich model.

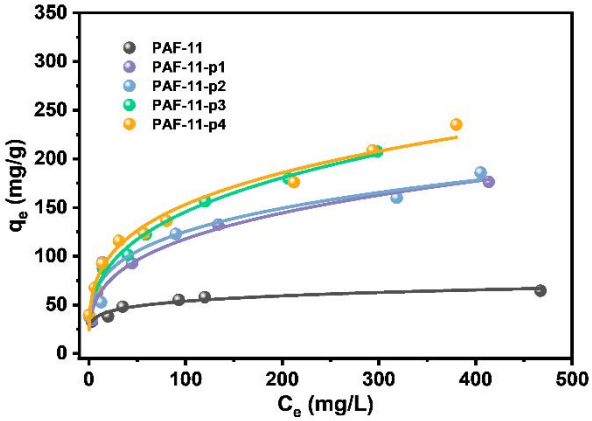

Supplementary Figure 21. MO adsorption isotherms by PAF-11 and corresponding partitioning PAFs analyzed through Freundlich model.

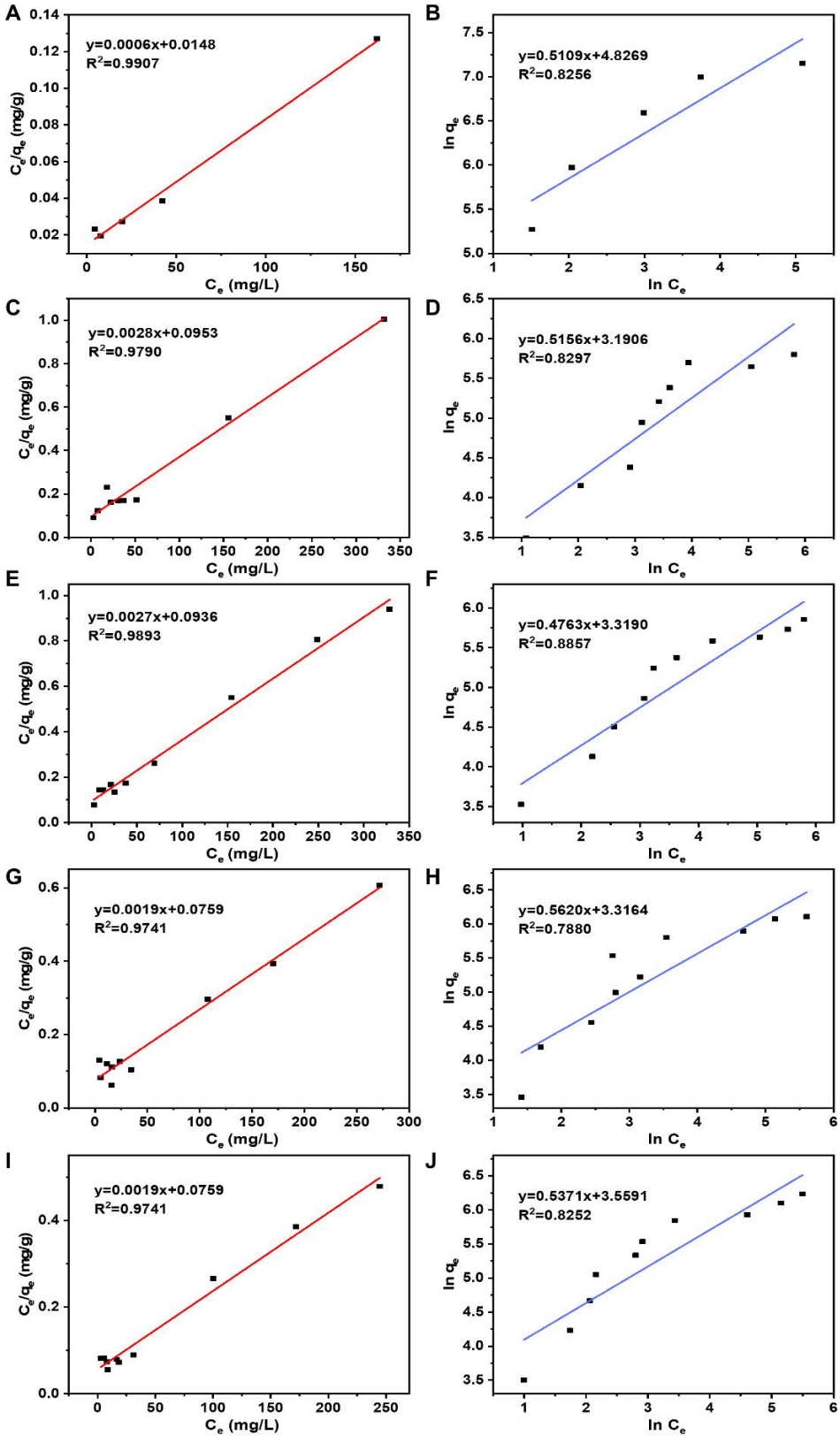

Supplementary Figure 22. Langmuir linear plots (Figures A, C, E, G, I) and Freundlich linear plots (Figures B, D, F, H, J) of AB for PAF-11 and corresponding partitioning PAFs.

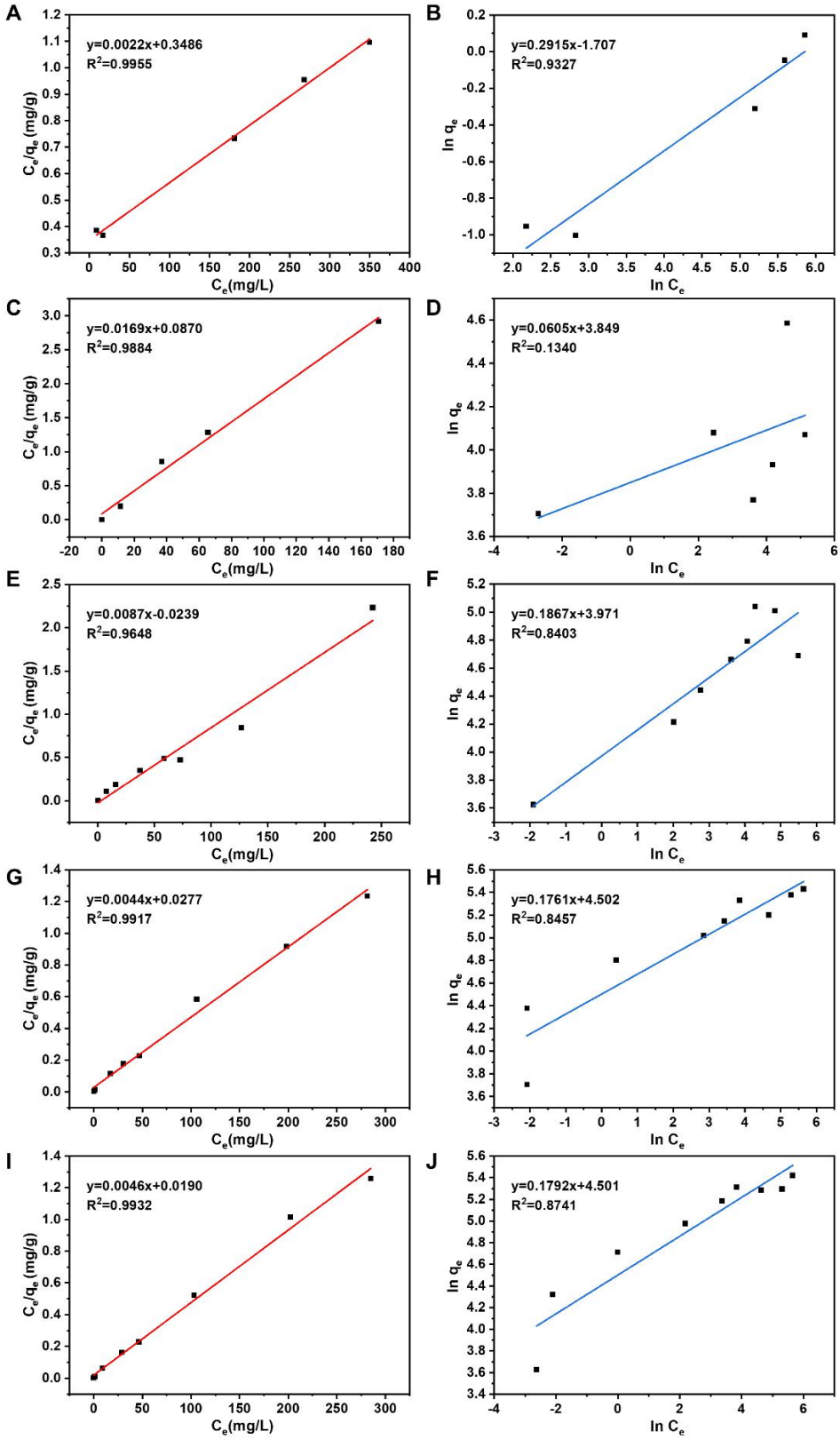

Supplementary Figure 23. Langmuir linear plots (Figures A, C, E, G, I) and Freundlich linear plots (Figures B, D, F, H, J) of RB for PAF-11 and corresponding partitioning PAFs.

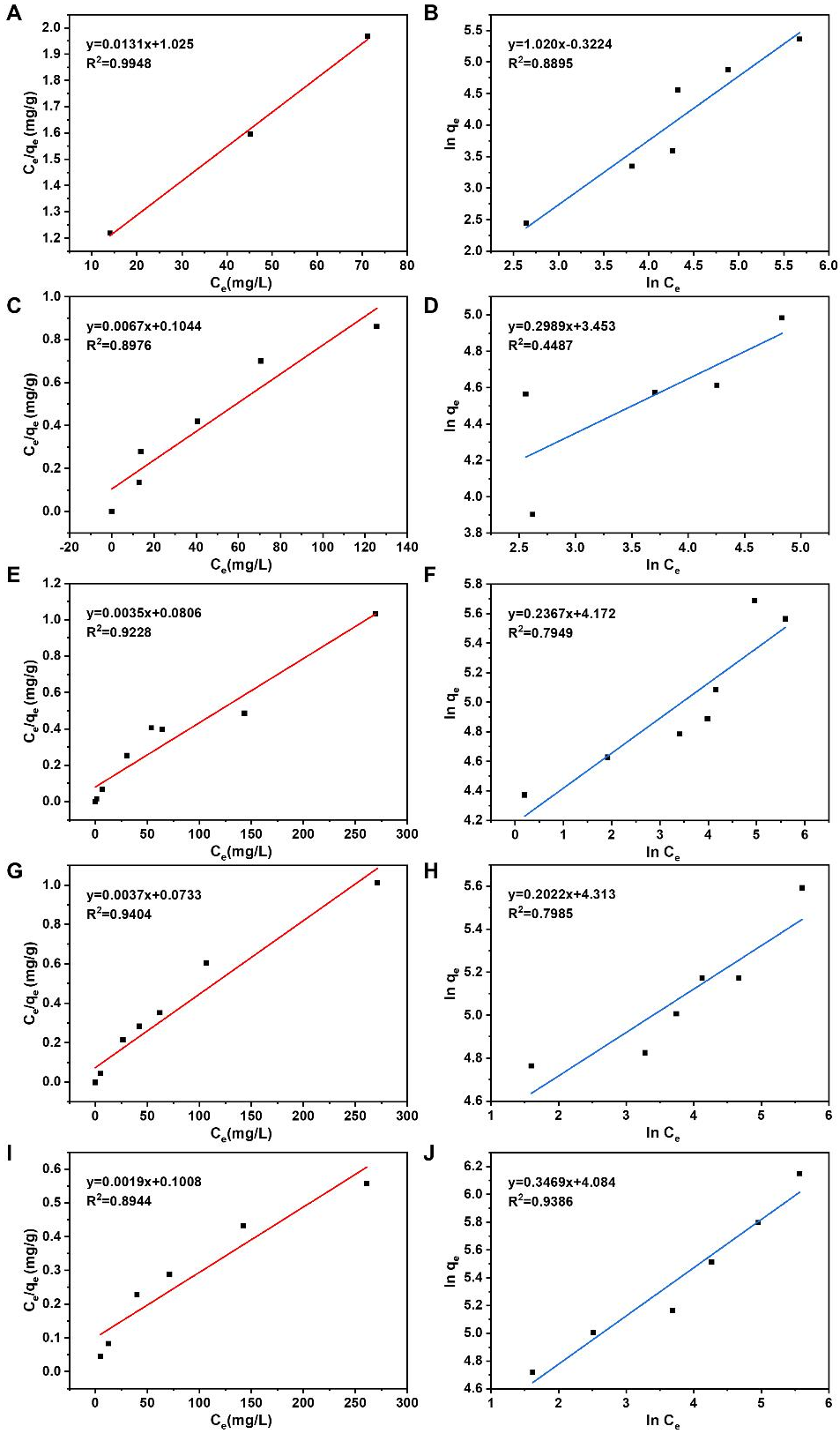

Supplementary Figure 24. Langmuir linear plots (Figures A, C, E, G, I) and Freundlich linear plots (Figures B, D, F, H, J) of MB for PAF-11 and corresponding partitioning PAFs.

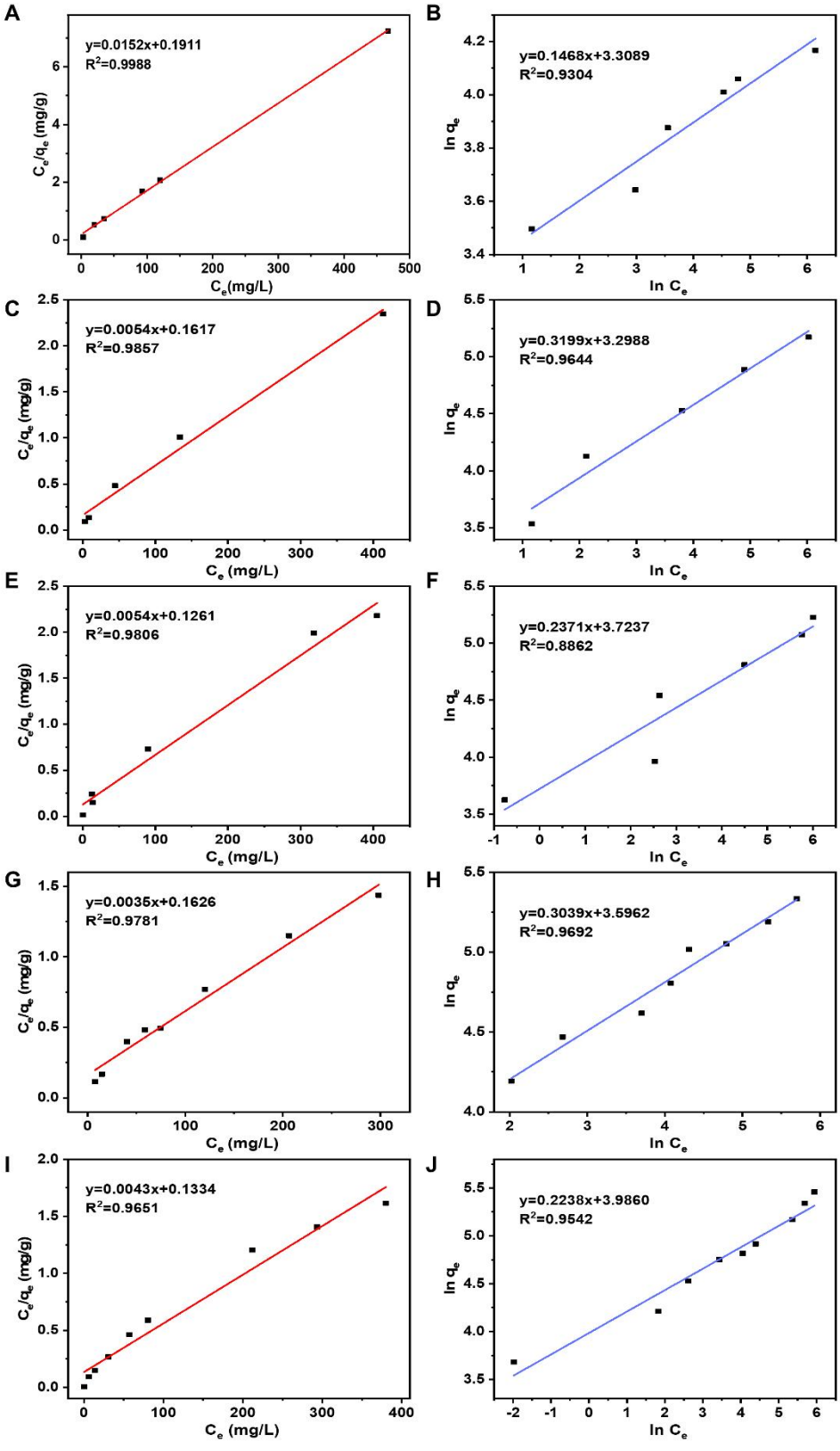

Supplementary Figure 25. Langmuir linear plots (Figures A, C, E, G, I) and Freundlich linear plots (Figures B, D, F, H, J) of MO for PAF-11 and its corresponding partitioning PAFs.

Supplementary Section 11. REFERENCES

1. Neshastehgar M, Rahmani P, Shojaei A, Molavi H. Enhanced adsorption removal performance of UiO-66 by rational hybridization with nanodiamond. *Micropor Mesopor Mat* 2020; 296: 110008. [DOI: 10.1016/j.micromeso.2020.110008]
2. Li R, Tang, X, Wu J, et al. A sulfonate-functionalized covalent organic framework for record-high adsorption and effective separation of organic dyes. *Chem Eng J* 2023; 464: 142706. [DOI: 10.1016/j.cej.2023.142706]
3. Haque E, Jun JW, Jhung SH. Adsorptive removal of methyl orange and methylene blue from aqueous solution with a metal-organic framework material, iron terephthalate (MOF-235). *J Hazard Mater* 2011; 185: 507-511. [DOI: 10.1016/j.jhazmat.2010.09.035]
4. Molavi H, Moghimi H, Taheri RA. Zr-Based MOFs with High Drug Loading for Adsorption Removal of Anti-Cancer Drugs: A Potential Drug Storage. *Appl Organomet Chem* 2020; 34: e5549. [DOI: 10.1002/aoc.5549 (acccessed 2024/01/31)]